Inorganic Chemistry

Article

pubs.acs.org/IC

Concerted Functions of Anions and Cations in a Molecular Ionic Crystal with Stable Three-Dimensional Micropores

Ryosuke Kawahara,[†] Sayaka Uchida,*[,†,§] and Noritaka Mizuno*[,‡]

[†]Department of Basic Sciences, School of Arts and Sciences, The University of Tokyo, 3-8-1 Komaba, Meguro-ku, Tokyo 153-8902, Japan

[‡]Department of Applied Chemistry, School of Engineering, The University of Tokyo, 7-3-1 Hongo, Bunkyo-ku, Tokyo 113-8656, Japan

[§]PRESTO, JST, 4-1-8 Honcho, Kawaguchi, Saitama 332-0012, Japan

Supporting Information

ABSTRACT: The molecular ionic crystal $[Cr_3O(OOCCH{=}CH_2)_6(H_2O)_3]_3[\alpha\text{-}PW_{12}O_{40}]\cdot 15H_2O$ [**Ia**] with stable three-dimensional micropores and a minimum aperture of 3.3 Å was synthesized with a phosphododecatungstate $[\alpha\text{-}PW_{12}O_{40}]^{3-}$ (polyoxometalate, POM) and a macrocation with acrylate ligands $[Cr_3O(OOCCH{=}CH_2)_6(H_2O)_3]^+$. The porous structure of **Ia** was basically constructed by an arrangement of macrocations forming a six-membered ring: vinyl groups ($CH{=}CH_2$) of adjacent macrocations were aligned parallel to each other, suggesting a weak dispersion force between them. A guest-free phase $[Cr_3O(OOCCH{=}CH_2)_6(H_2O)_3]_3[\alpha\text{-}PW_{12}O_{40}]$ [**Ib**] was formed by the treatment of **Ia** in vacuo at room temperature without any structure change. Compound **Ib** showed shape-selective sorption of CO_2 and C_2H_2 (molecular size = 3.3 Å) over N_2 (3.6 Å) and methane (3.7 Å), and the sorption enthalpy of C_2H_2 was larger than that of CO_2. The high affinity toward C_2H_2 was further confirmed as follows: the Monte Carlo simulations of the optimized geometries of C_2H_2 in **Ib** showed that both hydrogen atoms were in the vicinity of the surface oxygen atoms of POMs. The gas sorption profiles showed a much faster diffusion for C_2H_2. All these results suggest that the anion and cation mainly play the guest-binding and structure-directing roles, respectively, (i.e., concerted functions) in an ionic crystal with stable three-dimensional micropores.

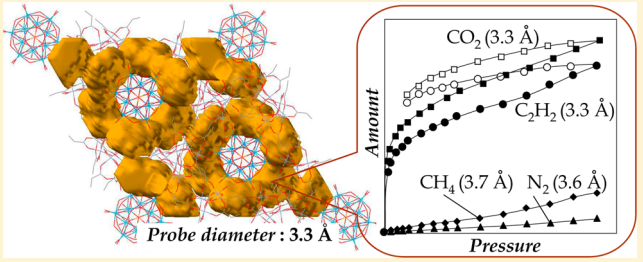

INTRODUCTION

Porous crystalline materials such as zeolites and metal organic frameworks (MOFs) have attracted great attention due to their wide range of applications in gas storage, separation of mixtures, ion-exchange, heterogeneous catalysis, etc.[1−6] On the other hand, ionic crystals (e.g., NaCl, CsCl) are normally nonporous because of the isotropic and long-range Coulomb interaction.[7] Recently, we and other research groups have reported that the use of molecular ions with appropriate elements, charges, sizes, shapes, or ligands enables the anisotropic packing and/or utilization of anisotropic interactions such as $\pi-\pi$ and hydrogen-bonding interactions, resulting in the formation of voids and channels in the crystal lattice.[8−12] Since the sizes of voids and channel apertures in the ionic crystals are generally small and similar to those of industrially important small inorganic and hydrocarbon gases, ionic crystals are potentially suitable for the storage and separation of these gases.[10,12] Moreover, ionic components as hosts can interact with guests through electrostatic interaction, which may assist to distinguish small differences in the physical properties of the guests.[9−12] Most importantly, specific functions (guest binding sites, catalytically active sites, etc.) that are incorporated beforehand into the ionic components could be maintained and utilized after the complexation, since they still exist as discrete molecules in the crystal lattice.

Polyoxometalates (POMs) are nanosized metal−oxide macroanions and are suited for the construction of porous ionic crystals in combination with molecular cations (macrocations).[11−19] POMs possess oxygen atoms on the molecular surface, which are potential guest binding sites through hydrogen-bonding or electrostatic interaction.[20,21] The use of macrocations with aromatic ligands as countercations of POMs induces one-dimensional assembly through $\pi-\pi$ interaction, and the resulting ionic crystals with one-dimensional channels show selective sorption of CO_2 and hydrocarbons.[12]

Zeolites and MOFs have large varieties of pore dimensions. For example, a mordenite zeolite with one-dimensional channels catalyzes the disproportionation of *m*-xylene via a transition state that is conformationally restricted,[22] while a faujasite zeolite with three-dimensional channels is suited for uniform guest diffusion and is utilized as a template to produce porous carbon.[23] On the other hand, to the best of our knowledge, there is only one example of an ionic crystal with a stable three-dimensional porous structure: a large molecular

Received: December 27, 2013
Published: March 28, 2014

   dx.doi.org/10.1021/ic4031574 | *Inorg. Chem.* 2014, 53, 3655−3661

cation with 12 aromatic ligands interacts with adjacent four cations through $\pi-\pi$ interaction to create three-dimensionally connected micropores, while the positions of the counteranion (NO_3^-) are highly disordered.[10]

To expand the chemistry of porous ionic crystals, we reached an idea to incorporate acrylate ligands ($CH{=}CH_2OOC^-$) in the macrocation to construct an ionic crystal with three-dimensional micropores. While it is well-recognized that dispersion force (i.e., $\pi-\pi$ interaction) between aromatic groups with multiple π-electrons and large planar molecular surfaces is suitable for constructing rigid one-dimensional structures,[12,24] construction of three-dimensional structures by utilizing vinyl groups has scarcely been reported: Shinkai and Takeuchi et al. have reported that a weak interaction between terminal olefin substituents of zinc-porphyrin hosts affects the guest recognition and pointed out the possibility of structure control in high-ordered architectures by utilizing this "olefin−olefin interaction".[25] Olefin moieties possess large flexibility, and such an "olefin−olefin interaction" may link multiple sites to construct stable three-dimensional structures.

In this work, a phosphododecatungstate, $[\alpha\text{-}PW_{12}O_{40}]^{3-}$, and a macrocation with acrylate ligands, $[Cr_3O(OOCCH{=}CH_2)_6(H_2O)_3]^+$, were used as molecular ionic components, and an ionic crystal, $[Cr_3O(OOCCH{=}CH_2)_6(H_2O)_3]_3[\alpha\text{-}PW_{12}O_{40}]\cdot 15H_2O$ [**Ia**], with three-dimensional micropores showing shape-selective guest sorption properties was obtained. *Stable three-dimensional micropores were constructed for the first time with discrete and precisely located molecular ionic components.* Detailed investigation of the crystal structure as well as Monte Carlo (MC) simulations and kinetic analyses of the guest sorption suggest that the anion and cation mainly play guest-binding and structure-directing roles, respectively, (i.e., concerted functions) in a porous ionic crystal.

EXPERIMENTAL METHODS

Syntheses. $Cr(NO_3)_3\cdot 9H_2O$ (0.025 mol, 10.0 g) and acrylic acid (0.05 mol, 3.6 g) were added to acetone (20 mL), and the solution was refluxed at 333 K for 5 h. The solution was filtered, 1,2-dichloroethane (280 mL) was added to the solute with stirring, and a green precipitate of $[Cr_3O(OOCCH{=}CH_2)_6(H_2O)_3](NO_3)\cdot nH_2O$ was formed (yield ca. 5 g). Mass spectrometry (MS) (fast atom bombardment (FAB), 3-nitrobenzyl alcohol) m/z: 598 $[Cr_3O(OOCCH{=}CH_2)_6]^+$, 616 $[Cr_3O(OOCCH{=}CH_2)_6(H_2O)]^+$, 634 $[Cr_3O(OOCCH{=}CH_2)_6(H_2O)_2]^+$, 652 $[Cr_3O(OOCCH{=}CH_2)_6(H_2O)_3]^+$.

$[Cr_3O(OOCCH{=}CH_2)_6(H_2O)_3](NO_3)\cdot nH_2O$ (3.0 mmol, 2.1 g) was added to distilled water (100 mL), and the solution was filtered to remove solid impurities. Acid-type POM $H_3PW_{12}O_{40}\cdot nH_2O$[26] (1.0 mmol, 2.9 g) was added to the solute, and green fine crystals of $[Cr_3O(OOCCH{=}CH_2)_6(H_2O)_3]_3[\alpha\text{-}PW_{12}O_{40}]\cdot 15H_2O$ [**Ia**] were formed (yield 2.0 g). The thermogravimetric (TG) analysis showed that 15 molecules of water of crystallization in **Ia** were completely desorbed by the evacuation or exposure to a dry N_2 flow at 298−305 K for more than 3 h, and the guest-free phase $[Cr_3O(OOCCH{=}CH_2)_6(H_2O)_3]_3[\alpha\text{-}PW_{12}O_{40}]$ [**Ib**] was formed (see Results and Discussion for the details). Elemental analysis (%) calcd for $[Cr_3O(OOCCH{=}CH_2)_6(H_2O)_3]_3[\alpha\text{-}PW_{12}O_{40}]\cdot 15H_2O$: C 12.71, H 2.01, P 0.61, Cr 9.17, W 43.22; found: C 12.40, H 2.20, P 0.64, Cr 9.10, W 42.90. Fourier transform−infrared (FT-IR) (KBr): 1647 (m, ν(C=C)), 1591 (s, ν_{as}(OCO)), 1446 (s, ν_s(OCO)), 1378 (m, δ(CH)), 1274 (s, ν(C−C)), 1077 (m, ν(P−O)), 983 (s, ν(W=O)), 895 (m, ν(W−Oc−W)), 821 (br, ν(W−Oe−W)) cm^{-1}.

Single-Crystal X-ray Structure Analyses. X-ray diffraction data of **Ia** were collected at 93 K with a CCD 2-D detector by using Rigaku Saturn diffractometer with graphite monochromated Mo Kα radiation. Structures were solved by direct method, expanded using Fourier techniques, and refined by full-matrix least-squares against F^2 with the SHELXTL package. Phosphorus, chromium, and tungsten atoms were refined anisotropically, while carbon and oxygen atoms were refined isotropically. Crystal data for **Ia**: trigonal $R\bar{3}$ (No. 148), a = 31.33(4), c = 21.84(3), V = 18568(40), Z = 6, 9472 reflections collected, 292 parameters, $R_1(I > 2\sigma(I))$ = 0.0933, wR_2 = 0.2345, GOF = 1.295, shift/error = 0.001. Void analyses of the crystal structures of **Ia**/**Ib** were carried out with the structure visualization program Mercury (CCDC).

Powder X-ray Diffraction Measurements. Powder X-ray diffraction (XRD) patterns were measured with XRD-DSCII (Rigaku Corporation) by using Cu Kα radiation (50 kV, 300 mA). Diffraction data were collected in the range of 2θ = 3−20° at 0.01° point, 5 s $step^{-1}$ at 303 K. The measurement for **Ib** was carried out under a dry N_2 flow.

Gas Sorption Measurements. Gas sorption isotherms were measured using a volumetric gas sorption apparatus Belsorp-max (BEL Japan Inc.) equipped with a cryostat BELCryo (BEL Japan Inc.) to control the temperature. Compound **Ia** (about 0.1 g) was treated in vacuo at 298 K for more than 3 h to form **Ib**. Sorption equilibrium was judged by the following criteria: ±0.3% of pressure change in 5 min. Sorption enthalpies ΔH_{abs} were calculated with the Clausius−Clapeyron equation.[27]

Time courses of the gas sorption were measured gravimetrically using a thermogravimetry/differential thermal analyzer Thermo Plus Evo (Rigaku). About 10 mg of fine crystals of **Ia** were well-ground and pretreated in a dry N_2 flow at 303 K for more than 3 h. A CO_2 or C_2H_2 gas was introduced into the apparatus with a four-way valve directly after the pretreatment.

Monte Carlo-Based Simulations. MC-based simulations were carried out using the Sorption tool of Materials Studio package (Accelrys Inc.) by the Metropolis MC method with universal forcefield.[28,29] Prior to the MC simulations, partial atomic charges of the constituent ions of **Ib** (phosphododecatungstates and macrocations) were derived from DFT calculations as follows: template structures (phosphododecatungstates and macrocations) were cut out from the crystal structure, and geometrical optimizations followed by Mulliken charge analysis[30] were carried out using the $Dmol^3$ tool[31] of Materials Studio package. The GGA-PBE exchange-correlation function[32] was used, electron spins of Cr^{3+} ions were treated in an unrestricted manner, and the double-numerical plus polarization (DNP) functions were used as the basis sets for all atoms. Molecular structures and partial atomic charges of guest molecules (CO_2 and C_2H_2) were also derived from the $Dmol^3$ tool.[12] Guest molecules were treated as rigid bodies, and only translational degrees of freedom were considered.

Solid-State Magic-Angle Spinning NMR Spectroscopy. Compound **Ia** (about 0.1 g) was placed in a Pyrex cylindrical glass cell, which was connected to a high-vacuum system. The glass cell was evacuated at 298 K for more than 3 h to form **Ib**. The resulting **Ib** was transferred directly into a small glass cell, which was sealed by firing. MAS NMR spectra were recorded with CMX-300 Infinity spectrometer (JEOL), and the resonance frequency was 121 MHz for ^{31}P. Single-pulse excitation was used, the MAS rate was 3 kHz, and $NH_4H_2PO_4$ (1.00 ppm) was used as an external standard for the calibration of chemical shifts.

RESULTS AND DISCUSSION

The crystal structure of $[Cr_3O(OOCCH{=}CH_2)_6(H_2O)_3]_3[\alpha\text{-}PW_{12}O_{40}]\cdot 15H_2O$ [**Ia**] is shown in Figure 1a. Compound **Ia** crystallized in a trigonal lattice and space group $R\bar{3}$ (No. 148). Macrocations were hexagonally packed in the *ab* plane, forming six-membered rings where POMs existed. Figure 1b shows the local structure of **Ia** in the *ab* plane. Vinyl groups of the acrylate ligands of macrocations were aligned parallel to each other with C−C distances of 3.75−3.85 Å, suggesting a weak dispersion force between the vinyl groups. While an interaction between terminal olefins was observed in a supramolecule,[25] to the best of our knowledge, this is *the first example of interaction between vinyl groups observed in a crystal structure*. The distances between

dx.doi.org/10.1021/ic4031574 | Inorg. Chem. 2014, 53, 3655−3661

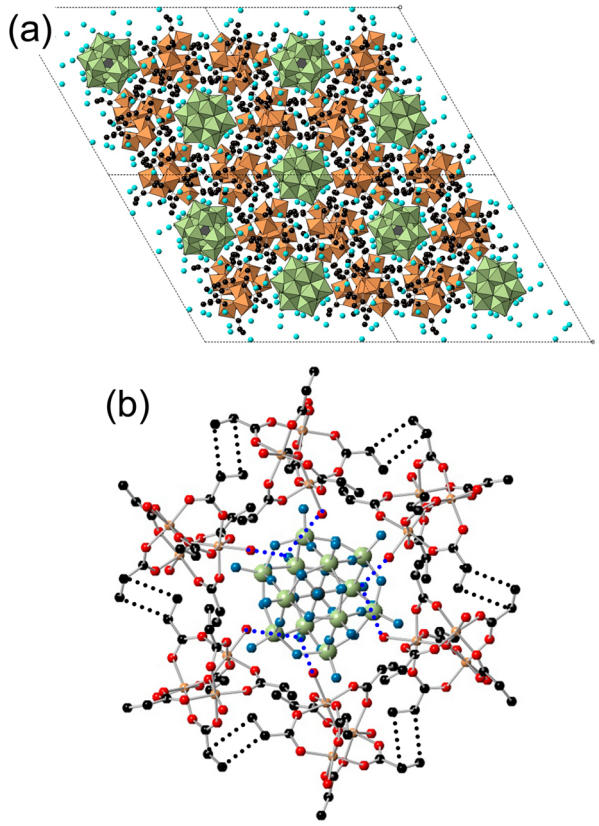

Figure 1. (a) Crystal structure of **Ia**. Light green and orange polyhedra show the $[WO_6]$ units of the phosphododecatungstates and $[CrO_6]$ units of the macrocation, respectively. Black and light blue spheres show the carbon atoms of the acrylate ligands and water of crystallization, respectively. (b) Local structure of **Ia** in the *ab* plane. Black, red, orange, blue, and light green spheres show the carbon, oxygen of the macrocation, chromium, oxygen of phosphododecatungstate, and tungsten atoms, respectively. Black and blue broken lines show the interaction between vinyl groups and hydrogen-bonding, respectively. Water of crystallization are omitted for clarity in (b).

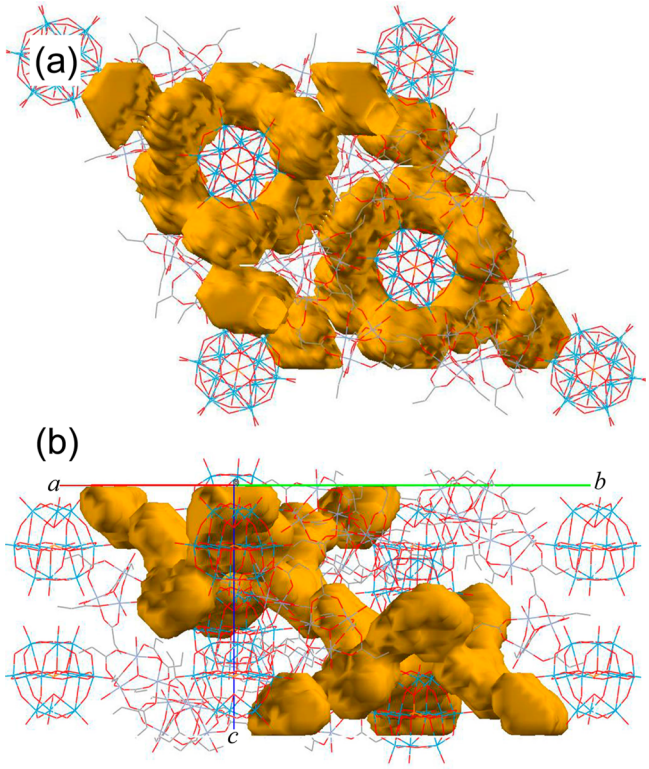

Figure 2. Void analyses of **Ia** with a probe diameter of 3.3 Å. Viewed (a) parallel and (b) perpendicular to the *ab* plane. Void spaces are shown in brown.

the oxygen atoms of the aqua ligands of the macrocation and those of the POM in the six-membered ring were 2.99−3.40 Å and were in hydrogen-bonding distances. Hydrogen-bonding interactions also existed among the macrocations arranged along the *c*-axis (3.27 Å).

The voids of **Ia** were analyzed with a probe diameter of 3.3 Å and are shown in Figure 2a. The void volume was 11.2% of the crystal lattice (2088 $Å^3$ per unit cell). Discrete voids existing around the POMs were interconnected with each other along the *c*-axis, resulting in a three-dimensional porous structure (Figure 2b). As shown in Supporting Information, Figure S1, the interconnection disappeared by the use of larger probe diameters (3.4 and 3.5 Å), suggesting that the minimum aperture of the interconnection is about 3.3 Å.

A weight loss of 5.4% (Supporting Information, Figure S2) was observed by the treatment of **Ia** in vacuo or under a dry N_2 flow at room temperature (298−303 K) for more than 3h, showing the complete desorption of water of crystallization in **Ia** by this treatment (calc. 5.3% for $15H_2O$). The powder XRD pattern of the resulting guest-free phase $[Cr_3O(OOCCH{=}CH_2)_6(H_2O)_3]_3[\alpha\text{-}PW_{12}O_{40}]$ [**Ib**] agreed well with that calculated for **Ia**, showing the maintenance of the porous structure after the desorption of water of crystallization (Figure 3).

Water sorption isotherms of **Ib** at 283, 288, 293, and 298 K are shown in Supporting Information, Figure S3a. The volume of water sorbed at the saturation (15 mol mol^{-1}) is about 2700 $Å^3$ per unit cell[33] and is comparable to the void volume of **Ib** (2780 $Å^3$) calculated with a probe diameter of 2.6 Å (i.e., the molecular size of water). Water sorption enthalpies were calculated with the Clausius−Clapeyron equation[27] and were plotted against the amounts of sorption (Supporting Information, Figure S3b). The water sorption enthalpies were initially low (22 kJ mol^{-1} at 1 mol mol^{-1}), gradually increased with increasing amounts of sorption, and almost reached the heat of condensation (44 kJ mol^{-1}) at high amounts of sorption (40 kJ mol^{-1} at 12 mol mol^{-1}). The small sorption enthalpy at low amounts of sorption is probably due to the energy consumption by small changes in the local arrangements of ionic components,[34,35] since water can strongly interact with the ionic components via hydrogen bonds. The powder XRD pattern of **Ib** after the sorption of water at 303 K and $P/P_0 \approx 1$ (Figure 3d) was analogous to those of **Ia** and **Ib** (Figures 3b and 3c), showing the maintenance of the porous structure after the water sorption.[36]

Supporting Information, Figure S4a shows the solid-state ^{31}P-MAS NMR spectrum of **Ib**. A peak appeared at −13.2 ppm accompanied by strong spinning side bands (SSBs). The position of the isotropic peak (−13.2 ppm) was confirmed by varying the MAS speed from 3 to 4 kHz. Since strong SSBs were not observed in the solid-state ^{31}P-MAS NMR spectra of $H_3[\alpha\text{-}PW_{12}O_{40}]\cdot nH_2O$ (n = 0−6),[20] the appearance of strong SSBs in the case of **Ib** is probably due to the paramagnetism of Cr(III).[37] Supporting Information, Figure S4b shows the solid-

dx.doi.org/10.1021/ic4031574 | Inorg. Chem. 2014, 53, 3655−3661

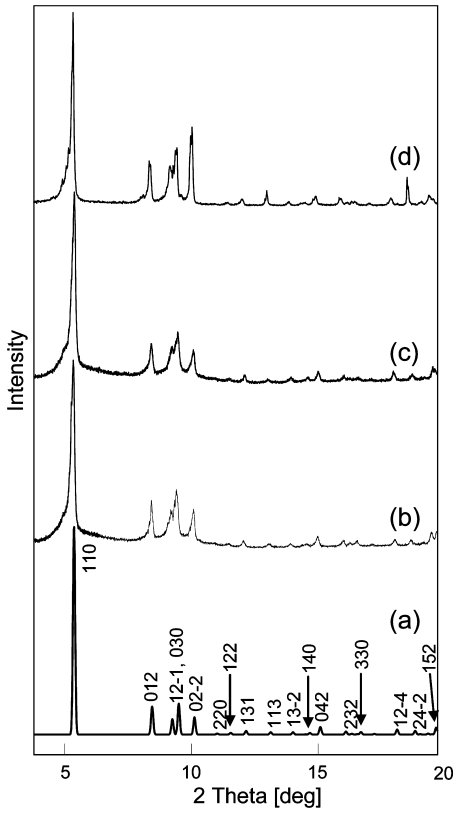

Figure 3. Powder XRD patterns of (a) **Ia** (calculated), (b) **Ia** (experimental), (c) **Ib** (experimental), and (d) **Ib** after the sorption of water at 303 K and $P/P_0 \approx 1$ (experimental). Figures in (a) show the Miller indices.

state ^{31}P-MASNMR spectrum of **Ia**. As compared with the spectrum of **Ib**, the line-shape narrowed, and the position of the isotropic peak changed to −15.0 ppm. The narrowing of the line-shape is probably due to the existence of diamagnetic water, which would decrease the effects of paramagnetism. The slight change in the position of the isotropic peak is probably due to the interaction of water with the surface oxygen atoms of POMs via hydrogen bonds.

Figure 4 shows the gas sorption isotherms of **Ib**. The molecular sizes of CO_2 and C_2H_2 are 3.3 Å[4] and are comparable to the minimum aperture of **Ib** (3.3 Å). The CO_2 and C_2H_2 isotherms at 198 K were type I of the IUPAC classification,

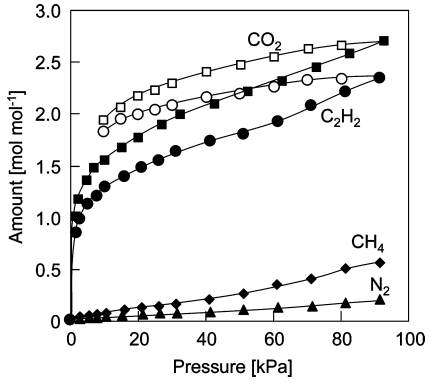

Figure 4. Gas sorption isotherms of CO_2 (198 K), C_2H_2 (198 K), CH_4 (115 K), and N_2 (77 K). Closed and open symbols show the sorption and desorption branches, respectively.

which are characteristic of microporous materials.[38] The volume of CO_2 and C_2H_2 sorbed at the saturation is about 1700 Å^3 per unit cell[39] and is less than 80% of the void volume of **Ib** (2088 Å^3) calculated with a probe diameter of 3.3 Å (i.e., the molecular size of CO_2 and C_2H_2).[40] The BET surface area calculated by the CO_2 sorption isotherm was ca. 50 m^2 g^{-1}. Hysteresis loops were observed in the CO_2 and C_2H_2 sorption−desorption isotherms; the loop in the C_2H_2 data was larger than that of CO_2, suggesting stronger interaction of C_2H_2 with the ionic components of **Ib**. The amounts of N_2 (77 K) and CH_4 (115 K) (Figure 4) were much smaller than those of CO_2 and C_2H_2, probably because the molecular sizes (N_2, 3.6 Å; CH_4, 3.7 Å)[4] are larger than the minimum aperture of **Ib** (3.3 Å). The results of the void analyses (Figure 2), powder XRD patterns (Figure 3), and gas sorption isotherms (Figure 4) show that stable three-dimensional micropores are constructed in the crystal lattice of **Ia**/**Ib**.

The CO_2 and C_2H_2 sorption enthalpies (1 mol mol^{-1} of sorption) calculated with the Clausius−Clapeyron equation[27] were 33 kJ mol^{-1} and 41 kJ mol^{-1}, respectively (Supporting Information, Figures S6 and S7). The larger sorption enthalpy of C_2H_2 is in line with the larger hysteresis loop in the C_2H_2 sorption−desorption isotherm (Figure 4). The CO_2 sorption enthalpy (33 kJ mol^{-1}) was smaller than those reported for various porous materials with strong CO_2 binding sites such as alkali metal ions and open metal sites (Supporting Information, Table S1, 36−59 kJ mol^{-1}). On the other hand, the C_2H_2 sorption enthalpy (41 kJ mol^{-1}) was rather large compared with those reported previously (Supporting Information, Table S2, 13−50 kJ mol^{-1}).

To investigate the states of CO_2 and C_2H_2 sorbed in **Ib**, MC-based simulations were carried out. Typical MC-based optimized geometries of CO_2 and C_2H_2 sorbed in **Ib** are shown in Figure 5a,b, respectively. Both CO_2 and C_2H_2 molecules existed in the vicinity of the POMs. The carbon atom of CO_2 was positively charged (+0.70 e)[12] and was in close distance (2.9−3.1 Å) with the negatively charged surface oxygen atoms of POMs (Figure 5c). Both hydrogen atoms of C_2H_2 were positively charged (+0.27 e)[12] and were in close distances (2.9−3.4 Å) with the negatively charged surface oxygen atoms of POMs (Figure 5d). These results suggest that the surface oxygen atoms of POMs function as guest binding sites and that the interaction between C_2H_2 and POM is strong because of the bidentate nature of C_2H_2.[41]

Time courses of the CO_2 and C_2H_2 sorption in **Ib** were measured gravimetrically at constant gas pressure (1 atm) and 303 K to investigate the sorption kinetics (Figure 6). The amounts of sorption increased and almost leveled off after about 2000 and 500 s for CO_2 and C_2H_2, respectively. Shorter time was taken to reach sorption equilibrium in the C_2H_2 sorption, which is probably due to the stronger host−guest interaction accelerating the uniform diffusion of C_2H_2 in the particle. The experimental data were analyzed by the Fickian diffusion model into spherical particles (eqs 1 and 2):[42]

$$\frac{\partial C}{\partial t} = D\left(\frac{\partial^2 C}{\partial r^2} + \frac{2}{r}\frac{\partial C}{\partial r}\right) \quad (1)$$

$$\frac{M_t}{M_\infty} = 1 - \frac{6}{\pi^2}\sum_{n=1}^{\infty}\frac{\exp(-Dn^2\pi^2 t/a^2)}{n^2} \quad (2)$$

Where C and r are the concentration of gases in the particle and radial coordinate, respectively. M_t, M_∞, a, and D are the

dx.doi.org/10.1021/ic4031574 | Inorg. Chem. 2014, 53, 3655−3661

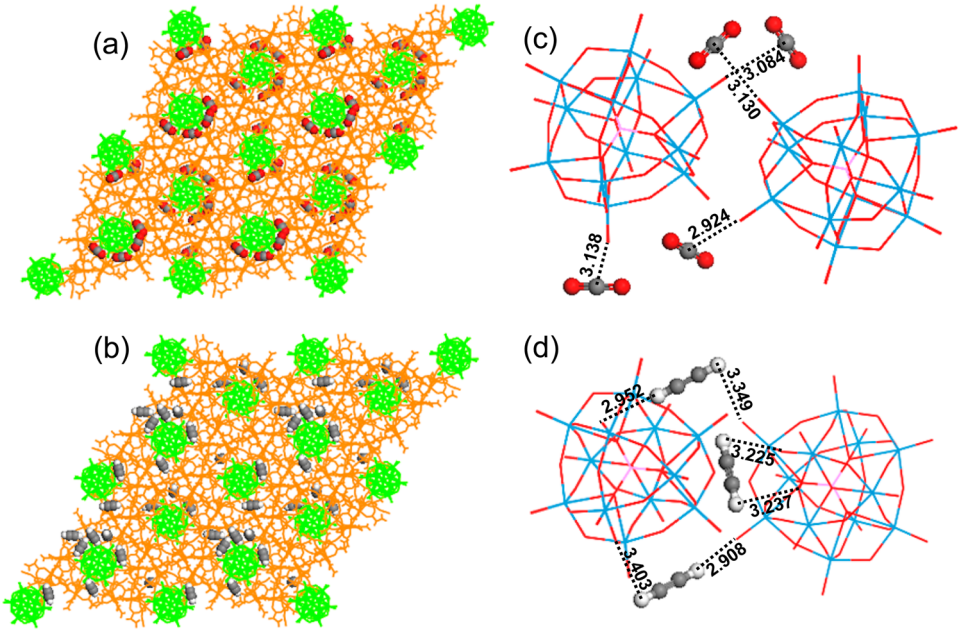

Figure 5. Typical optimized geometries of (a) CO_2 and (b) C_2H_2 sorbed in **Ib**. Typical local structures of phosphododecatungstate with (c) CO_2 and (d) C_2H_2. Green and orange molecules show the phosphododecatungstates and macrocations, respectively. Gray, white, and red atoms show the carbon, hydrogen, and oxygen atoms, respectively.

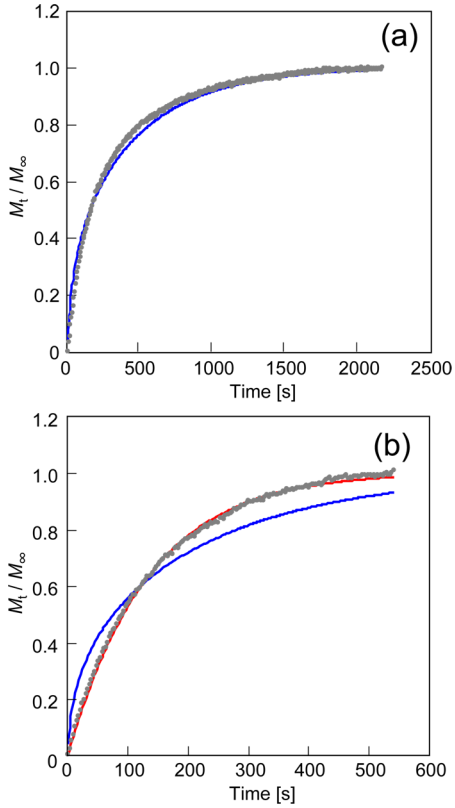

Figure 6. Time courses of (a) CO_2 and (b) C_2H_2 sorption in **Ib** at 303 K. The gray circles show the experimental data. The blue and red lines show the calculation with the Fickian diffusion and LDF model, respectively.

amounts of sorption at time t, amounts of sorption at equilibrium, particle size, and diffusion coefficient, respectively. As shown in Figure 6a, the experimental data for CO_2 was well-reproduced with a diffusion coefficient (D) of 2.0×10^{-12} cm^2 s^{-1}. This value is comparable to that of zeolite 4A (pore diameter 4 Å, $D = 8.1 \times 10^{-12}$ cm^2 s^{-1})[43] and is much smaller than those of zeolite 5A (pore diameter 5 Å, $D \approx 10^{-7}$ cm^2 s^{-1}) and MOF-5 (pore diameter 7.7 Å, $D \approx 10^{-5}$ cm^2 s^{-1}),[44] in line with the sizes of the channel apertures. On the other hand, the experimental data for C_2H_2 showed large deviation from the Fickian diffusion and was well-reproduced by the linear driving force (LDF) model (eqs 3 and 4):[45]

$$\frac{dM}{dt} = k(M_\infty - M_t) \tag{3}$$

$$\frac{M_t}{M_\infty} = 1 - \exp(-kt) \tag{4}$$

Where k is the rate constant. As shown in Figure 6b, the experimental data for C_2H_2 was well-reproduced with a rate constant (k) of 7.5×10^{-3} s^{-1}. While the Fickian diffusion model is suitable for simple diffusion processes, the LDF model has been well-adapted to various (ad)sorption processes, such as adsorption of inorganic gases on carbons and sorption of alcohol vapors in MOFs.[45,46] As suggested by the large hysteresis loop in the sorption−desorption isotherm (Figure 4), large sorption enthalpy (Supporting Information, Figure S7), and the bidentate nature of C_2H_2 (Figure 5d), the relatively strong interaction between C_2H_2 and POMs probably affects the sorption kinetics of C_2H_2.

Finally, the sorption properties of **Ib** were compared with our previous work. Ionic crystal $K_2[Cr_3O(OOCH)_6(4\text{-ethylpyridine})_3]_2[\alpha\text{-}SiW_{12}O_{40}]\cdot 2H_2O$ [**II**][47] possesses one-dimensional micropores with an aperture of 3.5 Å, and hydrated potassium ions (K^+) exist as guest binding sites. Ionic crystal $[Cr_3O(OOCCF_3)_6(H_2O)_3]_3[\alpha\text{-}PW_{12}O_{40}]\cdot 15H_2O$ [**III**][48] possesses two-dimensional layered structure with an interlayer distance of 3.5 Å. The inner surface of **III** is covered with the CF_3 groups, and the guests in the interlayer space interact with the inner surface via electrostatic interaction. We obtained a set of ionic crystals with similar compositions but different structure

dx.doi.org/10.1021/ic4031574 | Inorg. Chem. 2014, 53, 3655−3661

dimensionalities and guest binding sites by the synthesis and characterization of **Ib**.

The CO_2 sorption enthalpies (1 mol mol^{-1}) of **Ib** (Supporting Information, Figure S6), **II**,[47] and **III** (Supporting Information, Figure S8) were 33, 29, and 25 kJ mol^{-1}, respectively, and that of **Ib** was the largest. This is probably because, while **Ib** possesses negatively charged surface oxygen atoms of POMs as guest binding sites, hydration weakens the host (K^+)−guest (CO_2) interaction in **II**, and there are no specific guest binding sites in **III**. The time taken to reach equilibrium in the CO_2 sorption were 2000, 600, and 300 s, respectively, for **Ib** (Figure 6), **II**,[47] and **III** (Supporting Information, Figure S8), and the times decreased in line with the increase in the aperture sizes: **Ib** (pore size: 3.3 Å), **II** (pore size: 3.5 Å), and **III** (interlayer dimension: 3.5 Å × micrometer order).

CONCLUSION

Compound **Ia** with stable three-dimensional micropores and a minimum aperture of 3.3 Å was synthesized. The porous structure of **Ia** was constructed by an arrangement of macrocations forming a six-membered ring. The vinyl groups ($CH{=}CH_2$) of adjacent macrocations were aligned parallel to each other with C−C distances of ca. 3.8 Å, which is the first example of interaction between vinyl groups observed in a crystal structure. Guest-free phase **Ib** was formed by the treatment of **Ia** in vacuo at room temperature without any structure change. Compound **Ib** showed shape-selective sorption of CO_2 and C_2H_2 over N_2 and methane, and the sorption enthalpy of C_2H_2 was larger than that of CO_2. The high affinity toward C_2H_2 was further confirmed with Monte Carlo simulations and sorption profiles: the Monte Carlo simulations of the optimized geometries of guest molecules suggest that the surface oxygen atoms of POMs are guest binding sites and the bidentate nature of C_2H_2. The gas sorption profiles showed much faster diffusion for C_2H_2. All these results suggest that the anion and cation mainly play the guest-binding and structure-directing roles, respectively, (i.e., concerted functions) in the stable three-dimensional micropores of **Ib**.

ASSOCIATED CONTENT

Supporting Information

CIF data of **Ia**. CO_2 sorption enthalpies of various porous materials (Table S1). C_2H_2 sorption enthalpies of various porous materials (Table S2). Void analyses with larger probe diameters (Figure S1). Thermogravimetric analysis (Figure S2). Water sorption isotherms and enthalpies (Figure S3). Solid-state ^{31}P-MAS NMR spectroscopy (Figure S4). IR spectroscopy (Figure S5). CO_2 sorption isotherms and Clausius−Clapeyron plot (Figure S6). C_2H_2 sorption isotherms and Clausius−Clapeyron plot (Figure S7). CO_2 sorption properties of $[Cr_3O(OOCCF_3)_6(H_2O)_3]_3[\alpha\text{-}PW_{12}O_{40}]\cdot 15H_2O$ (Figure S8).This material is available free of charge via the Internet at http://pubs.acs.org.

AUTHOR INFORMATION

Corresponding Authors

*E-mail: csayaka@mail.ecc.u-tokyo.ac.jp. Phone: +81-3-5454-6601. Fax: +81-3-5454-6601. (S.U.)

*E-mail: tmizuno@mail.ecc.u-tokyo.ac.jp. Phone: +81-3-5841-7272. Fax: +81-3-5841-7220. (N.M.)

Notes

The authors declare no competing financial interest.

ACKNOWLEDGMENTS

This work was supported by JST-PRESTO, JSPS through its "Funding Program for World-Leading Innovative R&D on Science and Technology (FIRST Program), and Grants-in-Aid for Scientific Research from the Ministry of Education, Culture, Science, Sports, and Technology of Japan (MEXT).

REFERENCES

(1) Kuznicki, S. M.; Bell, V. A.; Nair, S.; Hillhouse, H. W.; Jacubinas, R. M.; Braunbarth, C. M.; Toby, B. H.; Tsapatsis, M. *Nature* **2001**, *412*, 720−724.

(2) Shang, J.; Li, G.; Singh, R.; Gu, Q.; Nairn, K. M.; Bastow, T. J.; Medhekar, N.; Doherty, C. M.; Hill, A. J.; Liu, J. Z.; Webley, P. A. *J. Am. Chem. Soc.* **2012**, *134*, 19246−19253.

(3) Kitagawa, S.; Kitaura, R.; Noro, S. *Angew. Chem., Int. Ed.* **2004**, *43*, 2334−2375.

(4) Li, J. R.; Kuppler, R. J.; Zhou, H. C. *Chem. Soc. Rev.* **2009**, *38*, 1477−1504.

(5) D'Alessandro, D. M.; Smit, B.; Long, J. R. *Angew. Chem., Int. Ed.* **2010**, *49*, 6058−6082.

(6) Furukawa, H.; Cordova, K. E.; O'Keeffe, M.; Yaghi, O. M. *Science* **2013**, *341*, 974−986.

(7) Shriver, D. F.; Atkins, P. W.; Langford, C. H. *Inorganic Chmistry*, 2nd ed.; Oxford University Press: Oxford, 1994.

(8) Bennett, M. V.; Beauvais, L. G.; Shores, M. P.; Long, J. R. *J. Am. Chem. Soc.* **2001**, *123*, 8022−8032.

(9) Takamizawa, S.; Akatsuka, T.; Ueda, T. *Angew. Chem., Int. Ed.* **2008**, *47*, 1689−1692.

(10) Cheng, X. N.; Xue, W.; Lin, J. B.; Chen, X. M. *Chem. Commun.* **2010**, *46*, 246−248.

(11) Uchida, S.; Hashimoto, M.; Mizuno, N. *Angew. Chem., Int. Ed.* **2002**, *41*, 2814−2817.

(12) Eguchi, R.; Uchida, S.; Mizuno, N. *Angew. Chem., Int. Ed.* **2012**, *51*, 1635−1640.

(13) Hill, C. L. Ed. Special Thematic Issue on Polyoxometalates, *Chem. Rev.* **1998**, *98*, 1-390.

(14) Liu, D.; Lu, Y.; Tan, H. Q.; Chen, W. L.; Zhang, Z. M.; Li, Y. G.; Wang, E. B. *Chem. Commun.* **2013**, *49*, 3673−3675.

(15) Todea, A. M.; Merca, A.; Bögge, H.; Glaser, T.; Pigga, J. M.; Langston, M. L. K.; Liu, T.; Prozorov, R.; Luban, M.; Schröder, C.; Casey, W. H.; Müller, A. *Angew. Chem., Int. Ed.* **2010**, *49*, 514−519.

(16) Mitchell, S. G.; Streb, C.; Miras, H. N.; Boyd, T.; Long, D. L.; Cronin, L. *Nature Chem.* **2010**, *2*, 308−312.

(17) Noro, S.; Tsunashima, R.; Kamiya, Y.; Uemura, K.; Kita, H.; Cronin, L.; Akutagawa, T.; Nakamura, T. *Angew. Chem., Int. Ed.* **2009**, *48*, 8703−8706.

(18) Mal, S. S.; Kortz, U. *Angew. Chem., Int. Ed.* **2005**, *44*, 3777−3780.

(19) Vasylyev, M. V.; Neumann, R. *J. Am. Chem. Soc.* **2004**, *126*, 884−890.

(20) Uchida, S.; Inumaru, K.; Misono, M. *J. Phys. Chem. B* **2000**, *104*, 8108−8115.

(21) Kimura, T.; Kamata, K.; Mizuno, N. *Angew. Chem., Int. Ed.* **2012**, *51*, 6700−6703.

(22) Csicsery, S. M. *Zeolites* **1984**, *4*, 202−213.

(23) Nishihara, H.; Kyotani, T. *Adv. Mater.* **2012**, *24*, 4473−4498.

(24) Zang, L.; Che, Y.; Moore, J. S. *Acc. Chem. Res.* **2008**, *41*, 1596−1608.

(25) Wakabayashi, R.; Ikeda, T.; Kubo, Y.; Shinkai, S.; Takeuchi, M. *Angew. Chem., Int. Ed.* **2009**, *48*, 6667−6670.

(26) Bailar, J. C., Jr. *Inorg. Synth.* **1939**, *1*, 132−133.

(27) Atkins, P. W. *Physical Chemistry;* Oxford University Press: Oxford, 1990.

(28) Metropolis, N.; Rosenbluth, A. W.; Rosenbluth, M. N.; Teller, A. H.; Teller, E. *J. Chem. Phys.* **1953**, *21*, 1087−1092.

(29) Rappé, A. K.; Casewit, C. J.; Colwell, K. S.; Goddard, W. A., III; Skiff, W. M. *J. Am. Chem. Soc.* **1992**, *114*, 10024−10035.
(30) Mulliken, R. S. *J. Chem. Phys.* **1955**, *23*, 1833−1840.
(31) Delley, B. *J. Chem. Phys.* **2000**, *113*, 7756−7764.
(32) Perdew, J. P.; Burke, K.; Ernzerhof, M. *Phys. Rev. Lett.* **1996**, *77*, 3865−3868.
(33) Calculated with the volume of a H_2O molecule (30.0 Å^3), which is estimated with the liquid density and molecular weight, the amount of H_2O (15 mol mol^{-1}), and the *Z* value of **Ia**/**Ib** (6).
(34) Uemura, K.; Kitagawa, S.; Fukui, K.; Saito, K. *J. Am. Chem. Soc.* **2004**, *126*, 3817−3828.
(35) Uchida, S.; Kawamoto, R.; Tagami, H.; Nakagawa, Y.; Mizuno, N. *J. Am. Chem. Soc.* **2008**, *130*, 12370−12376.
(36) The diffraction peaks of **Ib** slightly sharpened after the sorption of water, suggesting that hydrogen bonding between guest (water molecules) and host (POM and/or macrocation) probably assisted to improve the crystallinity of **Ib**.
(37) Bertini, I.; Luchinat, C. *Coord. Chem. Rev.* **1996**, *150*, 221−242.
(38) Gregg, S. J.; Sing, K. S. W. *Adsorption, Surface Area, and Porosity;* Academic Press: London, 1982.
(39) Calculated with the volume of a CO_2 molecule (102.5 Å^3), which is estimated with the liquid density and molecular weight, the amount of CO_2 at the saturation (2.7 mol mol^{-1}), and the *Z* value of **Ia**/**Ib** (6).
(40) The IR spectra of **Ib** after the sorption (of water, CO_2, or C_2H_2) were analogous to those of **Ia** (Supporting Information, Figure S5), showing that the molecular structures of the ionic components are maintained after the guest sorption.
(41) Matsuda, R.; Kitaura, R.; Kitagawa, S.; Kubota, Y.; Belosludov, R. V.; Kobayashi, T. C.; Sakamoto, H.; Chiba, T.; Takata, M.; Kawazoe, Y.; Mita, Y. *Nature* **2005**, *436*, 238−241.
(42) Crank, J. *The Mathematics of Diffusion;* Oxford University Press: London, 1956.
(43) *Handbook of Zeolite Science and Technology;* Auerbach, S. M., Carrado, K. A., Dutta, P. K, Eds.; CRC Press: Boca Raton, FL, 2003.
(44) Saha, D.; Bao, Z.; Jia, F.; Deng, S. *Environ. Sci. Technol.* **2010**, *44*, 1820−1826.
(45) Reid, C. R.; Thomas, K. M. *Langmuir* **1999**, *15*, 3206−3218.
(46) Fletcher, A. J.; Cussen, E. J.; Bradshaw, D.; Rosseinsky, M. J.; Thomas, K. M. *J. Am. Chem. Soc.* **2004**, *126*, 9750−9759.
(47) Eguchi, R.; Uchida, S.; Mizuno, N. *J. Phys. Chem. C* **2012**, *116*, 16105−16110.
(48) Uchida, S.; Kawahara, R.; Ogasawara, Y.; Mizuno, N. *Dalton Trans.* **2013**, *42*, 16209−16215.

dx.doi.org/10.1021/ic4031574 | *Inorg. Chem.* 2014, 53, 3655−3661